Surface-plasmon distributed-feedback quantum cascade lasers operating pulsed, room temperature

A. Bousseksou,[1,a)] Y. Chassagneux,[1] J. R. Coudevylle,[1] R. Colombelli,[1,b)] C. Sirtori,[2] G. Patriarche,[3] G. Beaudoin,[3] and I. Sagnes[3]
[1]*Institut d'Electronique Fondamentale, Université Paris Sud and CNRS, UMR8622, 91405 Orsay, France*
[2]*Laboratoire MPQ, Université Paris Diderot and CNRS, UMR7612, 75013 Paris, France*
[3]*Laboratoire de Photonique et de Nanostructures, CNRS/LPN, 91460 Marcoussis, France*

(Received 5 May 2009; accepted 16 July 2009; published online 3 September 2009)

We report distributed-feedback surface-plasmon quantum cascade lasers operating at $\lambda \approx 7.6$ μm. The distributed feedback is obtained by the sole patterning of the top metal contact on a surface plasmon waveguide. Single mode operation with more than 30 dB side mode suppression ratio is obtained in pulsed mode and at room temperature. A careful experimental study confirms that by varying the grating duty cycle, one can reduce the waveguide losses with respect to standard, unpatterned surface-plasmon devices. This allows one to reduce the laser threshold current of more than a factor of 2 in the 200–300 K temperature range. This approach may lead to a fabrication technology for midinfrared distributed-feedback lasers based on a very simple processing. © *2009 American Institute of Physics*. [DOI: 10.1063/1.3202765]

The quantum cascade (QC) laser is a semiconductor source for the midinfrared range of the electromagnetic spectrum ($2.75\ \mu m < \lambda < 24\ \mu m$).[1,2] Since its emission wavelength covers the "fingerprint" region of typical molecular absorptions, it is a device particularly interesting for spectroscopic applications. Single mode operation is therefore often required,[3] and the structure of choice to achieve this goal is the distributed feedback (DFB). Devices based on buried heterostructure gratings—together with advances in the design and technology of QC lasers—have led to the demonstration of single mode operation at room temperature (RT) at several wavelengths.[4–9] However, for applications requiring only pulsed RT operation, it is interesting to develop less technologically heavy solutions. This is the purpose of this paper, where a different approach relying on surface-plasmon QC lasers is analyzed.

It has been proposed, in fact, as a proof of principle[10] that a metal grating—alternating metal pads and air gaps—can operate as a frequency-selecting filter. In this paper we demonstrate that the presence of the grating induces a waveguide loss reduction and therefore pulsed, single mode operation at RT can be achieved by surface-plasmon QC lasers operating at $\lambda \approx 7.5$ μm. We have also performed a study of the device characteristics as a function of the grating duty cycle in order to identify the ideal operating range.

The model structure is a surface-plasmon QC laser where the top, unpatterned metallization is replaced with an air-metal grating whose period is Λ. We target operation at the first order Bragg condition, i.e., $\Lambda = \lambda / 2n_{\text{eff}}$, were n_{eff} and λ are, respectively, the effective optical index and the wavelength of the waveguide mode. The photonic band structure of the infinite grating system (see Fig. 1) has been calculated by solving the two dimensional Helmoltz equation in a single unit cell, i.e., one period of the grating, with Bloch periodic boundary conditions. The optical losses in the semiconductor layers are introduced using the Drude model (see Fig. 2, caption). The refractive index profile and the calculated eigenmodes profile intensity for a 50% duty cycle grating are shown in Figs. 1(c) and 1(d). The resulting photonic band structure in normalized frequency and wavevector units is shown in Fig. 2(a) for a 25%, 50%, and 70% duty-cycle grating (duty cycle 0 corresponds to no metallization). Only the region around the zone edge ($k_x = 0.5$) is shown, since the candidate modes for lasing are the ones close to the band edge, where states with almost zero group velocity appear.

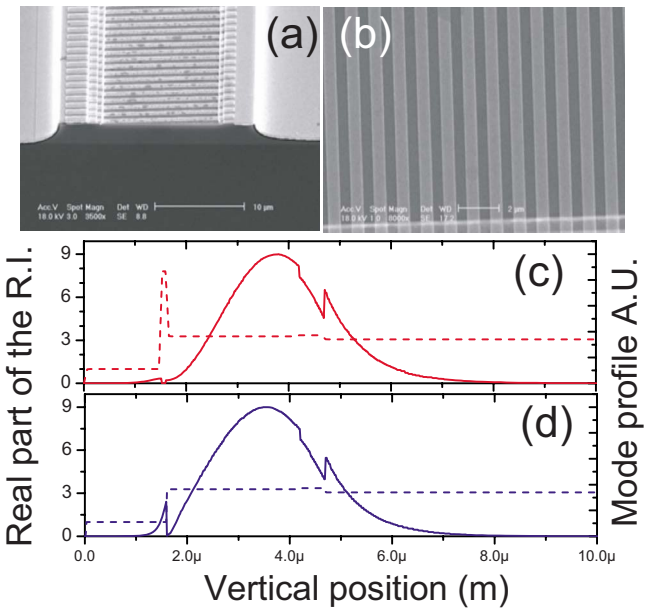

FIG. 1. (Color online) (a) Scanning electron microscopy (SEM) images of a typical device with a 50% duty-cycle grating. (b) Top-view SEM image of the metallic grating. (c) Calculated profile intensity for mode 2 (solid line) and real part of the refractive index (dashed line) for a 50% duty cycle DFB. Mode 2 exhibits field maxima below the metal fingers, therefore the reported one dimensional (1D) index profile corresponds to the metalized regions of the grating. (d) Calculated profile intensity for mode 1 (solid line) and real part of the refractive index (dashed line) for a 50% duty cycle DFB. Mode 1 exhibits field maxima below the air gaps, therefore the reported 1D index profile corresponds to the nonmetalized regions of the grating.

a)Electronic mail: adel.bousseksou@u-psud.fr.
b)Electronic mail: raffaele.colombelli@u-psud.fr.

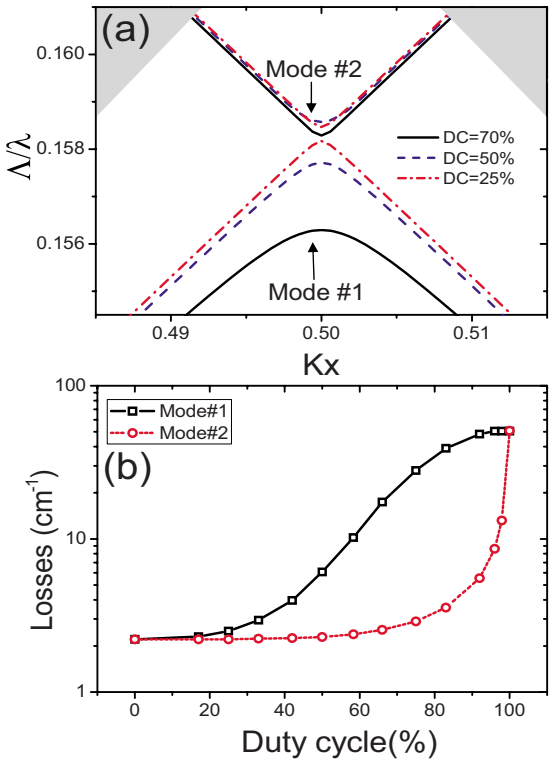

FIG. 2. (Color online) (a) Calculated photonic band structure around the band edge (k_x=0.5) for 70% (black continuous line), 50% (blue dashed line), and 25% (red dot-dashed line) grating duty cycles, showing the opening of a stop band. The grayed regions mark the zone above the substrate light line, where the calculated modes are not confined in the active region. (b) Calculated losses per unit of length (cm^{-1}) as a function of the grating duty cycle for the band edge states of panel (a). The refractive indexes of the layers composing the QC laser and used for the calculation are $n_{active\_region}=3.269+i*6.72\times10^{-5}$, $n_{InP\_substrate}=3.055+i*2.738\times10^{-4}$, $n_{InGaAs\_cladding}=3.345+i*2.342\times10^{-4}$, and $n_{gold}=7.8+i*54.6$. These values are obtained using a Drude model at a wavelength of 7.5 μm and with a constant scattering time of 0.15 ps. The active region is considered as a bulk layer, whose refractive index is averaged between the InGaAs wells and the AlInAs barriers.

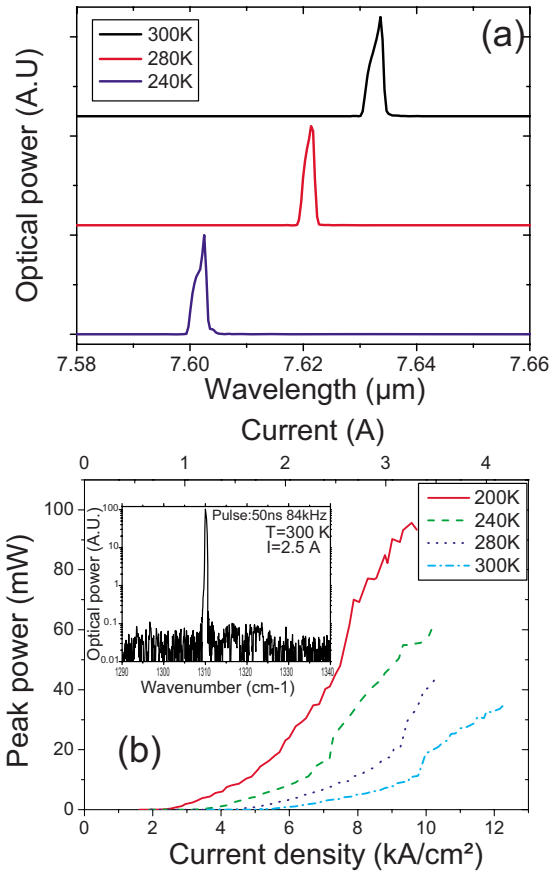

FIG. 3. (Color online) (a) Typical spectra of a SP DFB QC laser (50% grating duty cycle) at three heatsink temperatures. The spectra have been acquired in pulsed mode (100 ns at 84 kHz), using a Fourier transform infrared spectrometer operated in rapid-scan mode and equipped with a liquid-nitrogen-cooled MCT detector. We measure a wavelength shift with heatsink temperature of ≈0.4 nm/K. (b) Peak output power as a function of injected current for a 1480×23 μm^2 DFB QC laser operated at 240, 280, and 300 K, respectively. Inset: corresponding RT laser spectrum in semilogarithmic scale. The device exhibits a side mode suppression ration of 30 dB.

The band diagram of Fig. 2(a) proves that the sole metal periodic patterning provides enough feedback to introduce a stop band around the first order Bragg condition. For instance, at $\lambda=7.5$ μm the wavelength separation between the two calculated modes (labeled 1 and 2 in the rest of the paper), for a 25% duty-cycle grating, is ≈8 nm. The mode separation increases with the duty cycle up to a maximum of ≈190 nm (corresponding to ≈30 cm^{-1}), which is obtained for a 90% grating duty cycle. At higher dc values the mode splitting sharply decreases toward zero (the case of a pure surface-plasmon mode on an unpatterned surface[11]).

Figure 2(b) reports the calculated losses of the two candidate modes for lasing as a function of the grating duty cycle. Mode 1 exhibits almost monotonically increasing losses, while mode 2—the *low-loss mode*—exhibits stable low losses up to very high duty cycles of ≈80/85%. In theory therefore, mode 2 is particularly interesting for applications due to its stability with respect to possible grating fabrication errors. In addition, it was shown that when mode 2 is active the electric field maxima are located on top of the metal fingers, with useful applications to the generation of surface plasmons by electrical injection.[12,13]

The laser structure (InP281) is a surface-plasmon QC laser with target, nominal emission wavelength at $\lambda=7.5$ μm. It was grown in a low-pressure MOVPE (Metal Organic Vapor Phase Epitaxy) system and it contains 50 repeats of a four-well active region+injector QC heterostructure. Details can be found in Refs. 10 and 11. The epitaxy has been performed on *n*-doped InP substrates. The devices were processed as standard wet-etched laser ridges, typically 23 μm wide and a few millimeters long. The top metal contact (Ti/Au: 3/80 nm), as shown in Fig. 1, is patterned by lift off as a 25%, 50%, and 70% duty-cycle metal-air grating. Different grating periods Λ between 1.176 and 1.224 μm have been implemented.

Figure 3(a) shows the measured spectra of a 50% duty-cycle SP DFB laser operating at three different temperatures. The emission is single mode, and the measured wavelength tuning with the heatsink temperature is ≈0.4 nm/K. This value—which is much smaller than 1.2 nm/K, as measured on Fabry–Pérot devices fabricated with the same material—allows us to assign the feedback mechanism to the action of the grating. The grating superimposed on this device has a period of 1.212 μm. The emission wavelength at RT of ≈7.63 μm corresponds therefore to a normalized frequency $\Lambda/\lambda=0.1588$. This value is in good agreement with the calculated position of mode 2, as in the photonic band structure of Fig. 2(a). At constant temperature, changing the grating

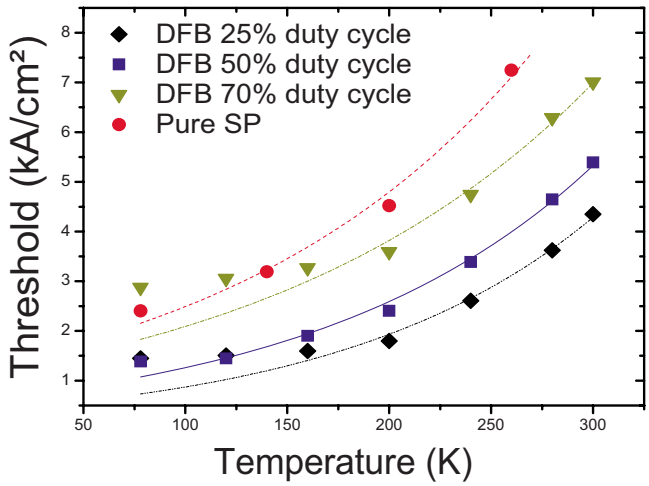

FIG. 4. (Color online) Laser threshold current density as a function of the heatsink temperature for a typical unpatterned surface-plasmon QC laser (red symbols) and for 25% (black symbols), 50% (blue symbols), 70% (dark yellow symbols) duty-cycle DFB lasers. The dotted lines are fits to the data with the fitting function $A\exp(T/T_0)$. T is the heatsink temperature and A and T_0 are fitting parameters. The T_0 values obtained for the unpatterned, 70%, 50%, and 25% grating duty cycle devices are, respectively, 152 ± 15, 165 ± 13, 138 ± 4, and 126 ± 9 K.

period allows one to match the grating resonances with the active material gain. The lasing mode can therefore be selected. In fact, for a device with $\Lambda=1.200$ μm a laser emission wavelength at RT of ≈7.66 μm was measured: this value corresponds to a normalized frequency $\Lambda/\lambda=0.1567$ and it matches the high frequency mode 1. At high injection currents ($J>10$ kA/cm^2) the laser emission typically becomes bimodal, or mode jumps are observed in some cases.

The output optical power as a function of injected current (L-I curve) of a typical 50% dc DFB laser is shown in Fig. 3(b). The output power was measured with a mercury-cadmium telluride (MCT) detector which had been calibrated with a thermopile. Pulsed RT operation (50 ns at 84 kHz) with a maximum peak power of ≈30 mW is achieved. The inset of Fig. 3(b) shows a typical spectrum acquired at a current density of ≈8 kA/cm^2. It shows single mode operation with a side mode suppression ratio of 30 dB.

Figure 4 reports the average current threshold as a function of the heatsink temperature for DFB lasers with 25%, 50%, and 70% dc gratings and $\Lambda=1.200$ μm. Data for an unpatterned surface-plasmon device (dc=100%) have been added for comparison. All the devices have been processed from the same wafer (InP281). In agreement with the calculations, the data show that patterning the top metal induces a loss reduction. All the patterned devices operate at RT in pulsed mode, while unpatterned surface-plasmon devices stop operating at a maximum heatsink temperature of ≈260 K. In the case of 25% and 50% duty cycle DFB devices, similar current thresholds are obtained for the modes labeled 1 and 2 (see Fig. 2). This confirms that at low duty cycles the two DFB modes have similar losses, and the laser can be made to operate on either modes by adjusting the grating period. On the other hand, spectral measurements show that only mode 2 is active (i.e., lasing) for 70% duty-cycle DFB devices. Since mode 2 always exhibits the lowest loss, the measured threshold variation as a function of the grating period in this case just reflects the overlap of the DFB mode with the QC material gain spectrum.

In conclusion we have shown that periodically patterning the top metal contact on surface-plasmon mid-IR QC lasers leads to single mode emission and to a threshold reduction. The mode selection mechanism has been theoretically modeled and the results are in good agreement with the experiments. The current threshold enhancement with respect to standard, unpatterned surface-plasmon devices allows one to achieve pulsed, RT single-mode operation with a 30 dB side mode suppression ratio. These devices could be suited to target applications only requiring pulsed, RT operation.

The authors would like to thank F. Julien, M. Carras, S. Laurent, and J. Teissier for useful discussions. The device fabrication has been performed at the CTU-IEF-Minerve which was partially funded by the "Conseil Général de l'Essonne." This work was conducted as part of a EURYI scheme award. See www.esf.org/euryi. This work was also supported by the French National Research Agency (program ANR-PNANO "MetalGuide").

[1] J. Devenson, O. Cathabard, R. Teissier, and A. N. Baranov, Appl. Phys. Lett. **91**, 251102 (2007).
[2] R. Colombelli, F. Capasso, C. Gmachl, A. L. Hutchinson, D. L. Sivco, A. Tredicucci, M. C. Wanke, A. M. Sergent, and A. Y. Cho, Appl. Phys. Lett. **78**, 2620 (2001).
[3] A. A. Kosterev and F. K. Tittel, IEEE J. Quantum Electron. **38**, 582 (2002).
[4] A. Wittmann, M. Giovannini, J. Faist, L. Hvozdara, S. Blaser, D. Hofstetter, and E. Gini, Appl. Phys. Lett. **89**, 141116 (2006).
[5] B. G. Lee, M. A. Belkin, R. Audet, J. MacArthur, L. Diehl, C. Pflügl, F. Capasso, D. C. Oakley, D. Chapman, A. Napoleone, D. Bour, S. Corzine, G. Hofler, and J. Faist, Appl. Phys. Lett. **91**, 231101 (2007).
[6] S. R. Darvish, W. Zhang, A. Evans, J. S. Yu, S. Slivken, and M. Razeghi, Appl. Phys. Lett. **89**, 251119 (2006).
[7] S. Blaser, D. A. Yarekha, L. Hvozdara, Y. Bonetti, A. Muller, M. Giovanni, and J. Faist, Appl. Phys. Lett. **86**, 041109 (2005).
[8] M. Carras and A. De Rossi, Phys. Rev. B **74**, 235120 (2006).
[9] M. Carras, M. Garcia, X. Marcadet, O. Parillaud, A. De Rossi, and S. Bansropun, Appl. Phys. Lett. **93**, 011109 (2008).
[10] A. Bousseksou, V. Moreau, R. Colombelli, C. Sirtori, G. Patriarche, O. Mauguin, L. Largeau, G. Beaudoin, and I. Sagnes, Electron. Lett. **44**, 807 (2008).
[11] M. Bahriz, V. Moreau, J. Palomo, R. Colombelli, D. A. Austin, J. W. Cockburn, L. R. Wilson, A. B. Krysa, and J. S. Roberts, Appl. Phys. Lett. **88**, 181103 (2006).
[12] A. Bousseksou, R. Colombelli, A. Babuty, Y. De Wilde, Y. Chassagneux, C. Sirtori, G. Patriarche, G. Beaudoin, and I. Sagnes, Opt. Express **17**, 9391 (2009).
[13] D. M. Koller, A. Hohenau, H. Ditlbacher, N. Galler, F. R. Aussenegg, A. Leitner, J. R. Krenn, S. Eder, S. Sax, and E. J. W. List, Appl. Phys. Lett. **92**, 103304 (2008).